Three New Polynuclear Bis(μ-phosphato) Vanadyl Clusters: $[HB(pz)_3VO(\mu\text{-}(C_6H_5O)_2PO_2)]_2$, $[HB(3,5\text{-}Me_2pz)_3VO(\mu\text{-}(C_6H_5O)_2PO_2)]\cdot C_7H_8$, and $H_2O\subset[t\text{-}Bupz(\mu\text{-}C_6H_5OPO_3)VO]_6(H_2O)_2\cdot 2CH_3CH_2OH$. Adaptability of the Cyclic $(OV)(OPO)_2(VO)$ Bridging Unit

Marcus R. Bond,† Ladd M. Mokry, Tom Otieno, Jeffrey Thompson, and Carl J. Carrano*

Department of Chemistry, Southwest Texas State University, San Marcos, Texas 78666

Received August 10, 1994[⊗]

The dinuclear complexes $[LVO(\mu\text{-}(C_6H_5O)_2PO_2)]_2$ (**I**) and $[L'VO(\mu\text{-}C_6H_5O)_2PO_2)]_2$ (**II**) (L = hydridotris(pyrazolyl)-borate; L′ = hydridotris(3,5-dimethylpyrazolyl)borate) and the hexanuclear complex $H_2O\subset[t\text{-}Bupz(\mu\text{-}C_6H_5\text{-}OPO_3)VO]_6(H_2O)_2\cdot 2CH_3CH_2OH$ (**III**) (*t*-Bupz = 3-*tert*-butylpyrazole) can be prepared by self-assembly of the components in solution under ambient conditions. These compounds have been characterized by UV−vis, IR, and EPR spectroscopies, magnetic susceptibility measurements, cyclic voltammetry, and X-ray structure determinations. Crystallographic parameters: for **I**, monoclinic, $P2_1/n$, a = 9.418(1) Å, b = 19.526(1) Å, c = 13.186(1) Å, β = 90.08(1)°, V = 2424.8(3) Å^3, Z = 2, T = 298 K, R = 0.0380, R_w = 0.0496, 2743 unique, observed ($|F| \geq 4\sigma(F)$) data, 316 least-squares parameters; for **II**, monoclinic, $P2_1/c$, a = 13.367(3) Å, b = 16.909(2) Å, c = 15.560(2) Å, β = 105.89(1)°, V = 3382.6(9) Å^3, Z = 2, T = 298 K, R = 0.0752, R_w = 0.0830, 2100 unique, observed ($|F \geq 4\sigma(F)$) data, 395 least-squares parameters; for **III**, monoclinic, $C2/c$, a = 25.750(4) Å, b = 15.171(2) Å, c = 27.537(5) Å, β = 95.00(1)°, V = 10716(2) Å^3, Z = 4, T = 298 K, R = 0.0687, R_w = 0.0699, 3216 unique, observed ($|F| \geq 4\sigma(F)$) data, 583 least-squares parameters. The structures of **I** and **II** consist of bis(μ-diphenyl phosphato-*O*,*O*′) divanadyl complexes in which the vanadyl oxygens of the two metal centers are oriented *anti* to one another. Compound **III** consists of a vaselike shell of μ-phenyl phosphato-*O*,*O*′,*O*″ vanadyl octahedra that encapsulate a molecule of water. The shell of this cluster is composed of fused, cyclic $(OV)(OPO)_2(VO)$ units such as those found at the core of the isolated dimeric species in **I** and **II**. This central bridging unit varies widely in its form in response to various structural forces. The presence of the sterically encumbered dimethylpyrazole groups in **II** forces a flattening of this central ring relative to that found in the unsubstituted dinuclear complex, **I**, while the presence of the template molecule in **III** generates four distinct bridging unit types in order to optimize interaction with the central water molecule and maintain the integrity of the cluster framework. Examination of the structures of the cyclic bridging units in these and other vanadyl phosphate systems shows that variation of the bridge structure can occur by (1) changing the coordination of the bridging phosphates in the equatorial planes of the metal centers or (2) changing the ring conformation through a continuous bending deformation. Structural variation is also reflected in the magnetic properties. Susceptibility measurements for the dinuclear complex **I** show weak ferromagnetic coupling (J/k = 3.3(4) K) while EPR measurements for the sterically encumbered dimethylpyrazolyl analog **II** indicate an uncoupled magnetic system. Antiferromagnetic coupling in the hexanuclear cluster is best fit to a model described by a pair of isolated divanadyl units (J/k = −14.4(3) K). These differences in exchange coupling among the three compounds can be explained by differences in the direct overlap of the vanadyl orbitals in the dinuclear bridging units.

Introduction

The structural and chemical properties of vanadyl phosphate systems continue to attract the attention of a growing audience of research scientists. The reasons for this are manifold. The wide-ranging structural variation within this class of compounds and, in many cases, the sensitivity of structure and stoichiometry to small changes in reaction conditions naturally appeal to one's curiosity. At the same time, the complicated architecture of many polyvanadyl species is often intriguing as well as aesthetically pleasing.[1] To magnetochemists this structural variation combined with the simple $S = {}^1/_2$ paramagnetism of the vanadyl (V=O) unit leads to a diversity of magnetic behavior that is useful for testing theoretical models.[2] Besides these basic research interests, there are a number of practical applications, both real and potential, that drive much of the current work in the field. Many compounds in the V−P−O family, $(VO)_2P_2O_7$ being a leading example, catalyze the oxidation of C_4 hydrocarbons to maleic acid.[3] Layered vanadyl organophosphonates, $VO(RPO_3)$, have importance as size-selective catalysts and sorbents.[4] Recently a growing series of discrete vanadium phosphate clusters were synthesized that are seen as potential hosts for inorganic supramolecular compounds.[5]

Our initial interest in the vanadium phosphate systems, however, differed from these. Since much of the work in our

* Author to whom correspondence should be addressed.
† Present address: Department of Chemistry, Southeast Missouri State University, Cape Girardeau, MO 63701.
⊗ Abstract published in *Advance ACS Abstracts,* March 1, 1995.

(1) Amoros, P.; Ibanez, R.; Beltran, A.; Beltran, D.; Fuertes, A.; Gomez-Romero, P.; Hernandez, E.; Rodriguez-Carvajal, J. *Chem. Mater.* **1991**, *3*, 407. Haushalter, R. C.; Wang, Z.; Thompson, M. E.; Zubieta, J. *Inorg. Chem.* **1993**, *32*, 3700.
(2) Villeneuve, G.; Amoros, P.; Beltran, D.; Drillon, M. In *Organic and Inorganic Low-Dimensional Crystalline Materials*; Delhaes, P., Drillon, M., Eds.; NATO ASI Series, Vol. B168; Plenum: New York, 1987.
(3) Johnston, D. C.; Johnson, J. W. *J. Chem. Soc., Chem. Commun.* **1985**, 1720 and references therein.
(4) Johnson, J. W.; Jacobson, A. J.; Butler, W. M.; Rosenthal, S. E.; Bordy, J. F.; Lewandowski, J. T. *J. Am. Chem. Soc.* **1989**, *111*, 381.
(5) Reuter, H. *Angew. Chem., Int. Ed. Engl.* **1992**, *31*, 1185.

0020-1669/95/1334-1894$09.00/0

laboratory concerns the biological role of vanadium, we have become interested in vanadium phosphate chemistry in regard to the interaction of vanadium complexes with biological phosphates, particularly with DNA. Vanadocene dichloride, for example, is well-known as an antitumor agent with a *cis*-dichloro structure similar to that of the widely studied *cis*-dichlorodiammineplatinum(II). Unlike the latter complex, however, vanadocene dichloride reacts with the phosphate backbone of DNA rather than at the organic bases.[6] These interests prompted us to prepare a number of V(III) and V(IV) complexes containing phosphate mono- and diesters in order to learn more about vanadium phosphate interactions and structure on a chemically simpler level.

In the course of this work, we have synthesized three new polynuclear vanadyl phosphate compounds, two dinuclear complexes, $[LVO(\mu\text{-}(C_6H_5O)_2PO_2)]_2$ (**I**) and $[L'VO(\mu\text{-}(C_6H_5O)_2PO_2)]_2$ (**II**) (L = hydridotris(pyrazolyl)borate; L′ = hydridotris(3,5-dimethylpyrazolyl)borate, and a hexanuclear complex, $H_2O\subset[t\text{-Bupz}(\mu\text{-}C_6H_5OPO_3)VO]_6(H_2O)_2{\cdot}2CH_3CH_2OH$ (**III**) (*t*-Bupz = 3-*tert*-butylpyrazole). Each of these compounds is formed via spontaneous self-assembly in solution under ambient conditions. While the structure and formation of the two dinuclear complexes are straightforward and easily rationalized, the structure of the hexanuclear compound is convoluted and the reasons for its preferential formation are not at all clear. In spite of these differences between the dinuclear and hexanuclear systems, close examination of their structures reveals a common structural motif, the cyclic bridging unit $(O{=}V)(OPO)_2(V{=}O)$. Several different conformations are found for this bridging core among the three compounds investigated here. This suggests a conformational flexibility for this bridging unit that enables it to adapt itself readily to a variety of structural situations. This adaptability, then, may play a major role in the formation and stability of vanadyl phosphate systems. As the pace and interest in this field intensify, we feel that now is an appropriate time to start systematically examining the variability and occurrence of this important structural element.

Experimental Section

Synthesis. (a) $[LVO(\mu\text{-}(C_6H_5O)_2PO_2)]_2$ (**I**). To 0.2011 g (0.5 mmol) of $HB(pz)_3VO(acac)$[7] dissolved in dry methylene chloride was added 1 equiv (0.1340 g) of diphenyl hydrogen phosphate (Aldrich). The pale violet solution was stirred overnight, during which time the color changed to blue. Filtration followed by evaporation of the solvent and recrystallization from toluene/hexane gave 0.2243 g (79.0%) of blue crystals. Anal. Calcd for $C_{44}H_{43}B_2N_{13}O_{10}P_2V_2$: C, 48.07; H, 3.94; N, 16.88. Found: C, 48.72; H, 3.84; N, 16.76. UV−vis, λ_{max} (ϵ): 750 nm (78.2). IR (cm^{-1}): $\nu_{V=O}$ = 972; ν_{B-H} = 2476; ν_{P-O} = 1276, 1116.

(b) $[L'VO(\mu\text{-}(C_6H_5O)_2PO_2)]_2$ (**II**). **II** was prepared analogously to **I** but starting with $HB(3,5\text{-}Me_2pz)_3VO(acac)$.[8] Recrystallization was from methylene chloride/toluene. UV−vis, λ_{max} (ϵ): 770 nm (71.6). IR (cm^{-1}): $\nu_{V=O}$ 968; ν_{B-H} = 2520; ν_{P-O} = 1279, 1200.

(c) $H_2O\subset[t\text{-Bupz}(\mu\text{-}C_6H_5OPO_3)VO]_6(H_2O)_2{\cdot}2CH_3CH_2OH$ (**III**). To $(t\text{-Bupz})_2VOCl_2$[9] (0.40 g, 1.10 mmol) was added 20 mL of water and the mixture stirred for several minutes, heated in a steam bath, and then filtered. To the blue filtrate was added 0.26 g (1.0 mmol) of the sodium salt of monophenyl phosphate, $C_6H_5OPO_3Na_2{\cdot}2H_2O$. The blue precipitate obtained was isolated, dried, and then recrystallized from ethanol. Yield: 0.11 g (15%). Anal. Calcd for $C_{82}H_{120}N_{12}V_6O_{35}P_6$: C, 42.35; H, 5.20; N, 7.23. Found: C, 42.01; H, 5.18; N 6.93. UV−vis, λ_{max} (ϵ): 774 nm (197.5), 648 (148.6). IR (cm^{-1}): $\nu_{V=O}$ = 959, 983; ν_{P-O} = 999, 1015, 1025, 1038. **III** can also be obtained from the reaction of $[(t\text{-Bupz})_4VO(H_2O)]Cl_2$[9] with $C_6H_5OPO_3Na_2{\cdot}2H_2O$.

X-ray Crystallography. Crystals (rectangular prism (**I**), blocklike (**II**), and platelike (**III**)) were sealed in Lindemann glass capillaries and mounted on a Siemens P4 diffractometer. Unit cell constants were determined by least-squares refinement of the angular settings of 12−30 well-centered, high-angle reflections. Data reduction, structure solution, and least-squares refinement were achieved using the SHELXTL-PLUS crystallographic software[10] from Siemens. Pertinent parameters regarding crystal data, data collection, and structure solution and refinement are summarized in Table 1 for each compound. Details of the individual structure refinements are summarized below.

(a) $[LVO(\mu\text{-}(C_6H_5O)_2PO_2)]_2$ (**I**). Structure solution was achieved *via* direct methods; the subsequent structure refinement proceeded normally. Anisotropic thermal parameters were refined for all non-hydrogen atoms. Positions of the hydrogen atoms were calculated to give an idealized geometry and then fixed to ride on their respective bound atoms. A fixed, isotropic thermal parameter (0.08 Å^2) was assigned to each hydrogen. Final refinement of 316 least-squares parameters against 2743 unique, observed ($F \geq 4\sigma(F)$) reflections gave agreement factors R = 0.0380 and R_w = 0.0496 and excursions on the difference map between −0.28 and 0.20 e/Å^3. Atomic coordinates are listed in Table 2; vanadyl coordination bond lengths and angles are listed in Table 3. A thermal ellipsoid plot of the molecule with the atomic labeling scheme is presented in Figure 1.

(b) $[L'VO(\mu\text{-}(C_6H_5O)_2PO_2)]_2{\cdot}C_7H_8$ (**II**). Structure solution was achieved *via* direct methods with most of the non-hydrogen atoms found on the *E* map. The remaining non-hydrogen atoms were located on electron density difference maps during the least-squares refinement. Several difference map peaks were found on or about an inversion center and isolated from the divanadyl species. These were interpreted as a 2-fold disordered toluene of crystallization and were included in the refinement with the C−C bond lengths constrained to a common value (1.39(4) Å). Anisotropic thermal parameters were refined for all non-hydrogen atoms except for those in the cocrystallized toluene. Positions of the hydrogen atoms were calculated to give an idealized geometry and then fixed to ride on their respective bound atoms. Hydrogen atom positions were not calculated for the disordered toluene. Common, isotropic thermal parameters were refined for groups of hydrogen atoms. The position of the hydride bound to boron was found on the difference map and included in the early stages of refinement, but with its coordinates fixed during the last stages. Hydride scattering factors and a small, isotropic thermal parameter were assigned to this atom. Final refinement of 395 least-squares parameters against 2100 unique, observed ($F > 4\sigma(F)$) reflections gave agreement factors R = 0.0752 and R_w = 0.0830 and excursions on the difference map between −0.44 and 0.55 e/Å^3. Atomic coordinates are listed in Table 4; vanadyl coordination bond lengths and angles are listed in Table 3. A thermal ellipsoid plot of the molecule with the atomic labeling scheme is presented in Figure 1.

(c) $H_2O\subset[t\text{-Bupz}(\mu\text{-}C_6H_5OPO_3)VO]_6(H_2O)_2{\cdot}2CH_3CH_2OH$ (**III**). Structure solution was achieved *via* direct methods with most of the non-hydrogen atoms found on the *E* map. The remaining non-hydrogen atoms were located on electron density difference maps during the least-squares refinement. Anisotropic thermal parameters were refined for all non-hydrogen atoms. Large, elongated thermal parameters found for the carbon atoms of the phenyl ring bound to O(51) were interpreted as evidence of 2-fold disorder of the ring. Estimated positions of the atoms for the two orientations were entered into the refinement with both rings constrained to ride on O(51) with the ring atoms fixed in a hexagon (C−C = 1.395 Å). Site occupation factors for the two orientations were refined with the sum of the factors constrained to 1.0. Anisotropic thermal parameters were not refined for the disordered pair. In order to reduce the number of parameters, the remaining phenyl

(6) Toney, J. H.; Brock, C. P.; Marks, T. J. *J. Am. Chem. Soc.* **1986**, *108*, 7263.
(7) Mohan, M.; Holmes, S. M.; Butcher, R. J.; Jasinski, J. P.; Carrano, C. J. *Inorg. Chem.* **1992**, *31*, 2029.
(8) Hunt, K. E.; Spartalian, K.; Derusha, M.; Nunn, C. M.; Carrano, C. J. *Inorg. Chem.* **1989**, *28*, 4392.
(9) Mohan, M.; Bond, M. R.; Otieno, T.; Carrano, C. J. *Inorg. Chem.*, in press.
(10) Sheldrick, G. M. *SHELXTL-PC*, Version 4.1; Siemens X-ray Analytical Instruments, Inc.: Madison, WI, 1989. Scattering factors were from: *International Tables for X-ray Crystallography*; Ibers, J., Hamilton, W., Eds.; Kynoch: Birmingham, England, 1974; Vol. IV.

Table 1. Summary of Crystallographic Data and Data Collection Parameters for **I**–**III**

parameter	I	II	III
formula	$C_{42}H_{40}B_2N_{12}O_{10}P_2V_2$	$C_{36}H_{64}B_2N_{12}O_{10}P_2V_2$	$C_{82}H_{120}N_{12}O_{35}P_6V_6$
space group	$P2_1/n$	$P2_1/c$	$C2/c$
temp, K	298	298	298
a, Å	9.418(1)	13.367(3)	25.750(4)
b, Å	19.526(1)	16.909(2)	15.171(2)
c, Å	13.186(1)	15.560(2)	27.537(5)
α, deg	90.00	90.00	90.00
β, deg	90.08(1)	105.89(1)	95.00(1)
γ, deg	90.00	90.00	90.00
V, Å^3	2424.8(3)	3382.6(9)	10716(2)
ϱ_{calc}, g cm^{-3}	1.449	1.287	1.441
Z	2	2	4
fw	1058.3	1310.7	2325.4
cryst size, mm	0.3 × 0.4 × 0.7	0.2 × 0.4 × 0.5	0.2 × 0.4 × 0.6
μ, cm^{-1}	5.20	3.86	6.74
radiation	graphite-monochromated Mo Kα (λ = 0.710 73 Å)		
scan type	θ–2θ	θ–2θ	θ–2θ
data collection range, deg	4–47.5	3.5–45	3.5–45
R_{merge}	0.0859	0.0405	0.0169
no. unique data	3682	4342	6910
no. obs data	2743	2100	3216
data:param ratio	8.7:1	5.3:1	5.5:1
transm	0.8297/0.8924	0.8300/0.8920	0.852/0.903
R^a	0.0380	0.0752	0.0687
$R_w{}^a$	0.0496	0.0830	0.0699
max diff peak, e/Å^3	0.20	0.55	0.44
Δ/σ(max)	0.000	0.031	0.006

[a] Quantity minimized: $\omega w(F_o - F_c)^2$. $R = \sum|F_o - F_c|/\omega F_o$. $R_w = (\omega w(F_o - F_c)^2/\sum(wF_o)^2)^{1/2}$.

Table 2. Atomic Coordinates ($\times 10^4$) and Equivalent, Isotropic Thermal Parameters (Å^2 × 10^3) for $[LVO(\mu\text{-}(C_6H_5O)_2PO_2)]_2$ (**I**)

atom	x	y	z	U(eq)[a]
V(1)	5008(1)	1214(1)	513(1)	31(1)
P(1)	5066(1)	334(1)	−1548(1)	33(1)
O(1)	6673(3)	1106(1)	407(2)	49(1)
O(2)	4447(3)	361(1)	1257(2)	41(1)
O(3)	4334(3)	772(1)	−786(2)	37(1)
O(4)	4045(3)	232(1)	−2499(2)	43(1)
O(5)	6358(3)	769(1)	−1959(2)	43(1)
B(1)	3453(5)	2638(2)	1257(3)	47(2)
N(1)	2671(3)	1479(2)	718(2)	41(1)
N(2)	2286(3)	2115(2)	1046(2)	43(1)
C(11)	1472(4)	1133(2)	564(3)	53(1)
C(12)	305(4)	1543(3)	799(3)	64(2)
C(13)	867(4)	2154(2)	1099(3)	55(2)
N(3)	4920(3)	2182(1)	−200(2)	38(1)
N(4)	4292(3)	2730(1)	255(2)	43(1)
C(14)	5389(4)	2397(2)	−1097(3)	46(1)
C(15)	5068(5)	3082(2)	−1232(3)	57(2)
C(16)	4365(5)	3272(2)	−368(3)	56(2)
N(5)	5148(3)	1744(2)	1899(2)	39(1)
N(6)	4456(3)	2346(2)	2065(2)	43(1)
C(17)	5924(4)	1612(2)	2728(3)	52(1)
C(18)	5730(5)	2128(3)	3435(3)	64(2)
C(19)	4798(5)	2573(2)	2999(3)	59(2)
C(21)	3661(4)	770(2)	−3151(3)	39(1)
C(22)	3118(4)	1380(2)	−2800(3)	46(1)
C(23)	2757(4)	1879(2)	−3500(4)	58(2)
C(24)	2938(5)	1769(3)	−4519(4)	65(2)
C(25)	3447(5)	1151(3)	−4856(3)	69(2)
C(26)	3809(4)	650(2)	−4172(3)	55(2)
C(31)	7632(4)	487(2)	−2320(3)	42(1)
C(32)	7685(4)	211(2)	−3271(3)	60(2)
C(33)	8968(6)	−35(3)	−3629(4)	78(2)
C(34)	10152(5)	6(3)	−3045(5)	79(2)
C(35)	10090(5)	291(3)	−2096(4)	77(2)
C(36)	8815(5)	535(2)	−1723(3)	60(2)

[a] Equivalent isotropic U defined as one-third of the trace of the orthogonalized U_{ij} tensor.

rings were also fixed to ride on their respective bound oxygens. Positions of the hydrogen atoms were calculated to give an idealized geometry; positions for those bound to oxygen atoms were taken from the difference map and then fixed to ride on their respective bound atoms with isotropic thermal parameters fixed at 0.12 Å^2. Final refinement of 583 least-squares parameters against 3216 unique, observed ($F \geq 4\sigma(F)$) reflections gave agreement factors $R = 0.0687$ and $R_w = 0.0699$ and excursions on the difference map between −0.42 and 0.44 e/Å^3. Atomic coordinates are listed in Table 5; vanadyl coordination bond lengths and angles are listed in Table 6. A thermal ellipsoid plot of the molecule with the atomic labeling scheme is presented in Figure 2.

Table 3. Pertinent Bond Lengths (Å) and Angles (deg) for $[LVO(\mu\text{-}C_6H_5O)_2PO_2)]_2$ (**I**) and $[L'VO(\mu\text{-}(C_6H_5O)_2PO_2)]_2{\cdot}C_7H_8$ (**II**)

	I[a]	II[b]
V(1)–V(1A)	4.931(1)	5.369(4)
V(1)–O(1)	1.588(2)	1.591(7)
V(1)–O(2)	2.005(2)	2.007(6)
V(1)–O(3)	2.020(2)	2.025(8)
V(1)–N(1)	2.278(3)	2.327(8)
V(1)–N(3)	2.111(3)	2.118(8)
V(1)–N(5)	2.105(3)	2.097(10)
	I	**II**
O(1)–V(1)–O(2)	101.1(1)	98.6(3)
O(1)–V(1)–O(3)	100.2(1)	98.7(4)
O(2)–V(1)–O(3)	88.7(1)	89.7(3)
O(1)–V(1)–N(1)	174.2(1)	176.2(3)
O(2)–V(1)–N(1)	82.8(1)	84.1(3)
O(3)–V(1)–N(1)	84.0(1)	83.9(3)
O(1)–V(1)–N(3)	96.8(1)	95.0(3)
O(2)–V(1)–N(3)	162.0(1)	165.9(3)
O(3)–V(1)–N(3)	89.6(1)	91.8(3)
N(1)–V(1)–N(3)	79.2(1)	82.2(3)
O(1)–V(1)–N(5)	94.7(1)	95.4(4)
O(2)–V(1)–N(5)	90.0(1)	90.2(3)
O(3)–V(1)–N(5)	165.0(1)	165.7(3)
(1)–V(1)–N(5)	81.1(1)	81.9(3)
N(3)–V(1)–N(5)	87.1(1)	85.0(3)

[a] Symmetry key: A = 1 − x, −y, −z. [b] Symmetry key: A = −x, −y, −z.

Magnetic Susceptibility Measurements. Room-temperature solid-state susceptibilities were measured for finely ground samples using a Johnson-Mathey MSB-1 susceptibility balance. Solution susceptibility data were measured at room temperature *via* the Evans method[11]

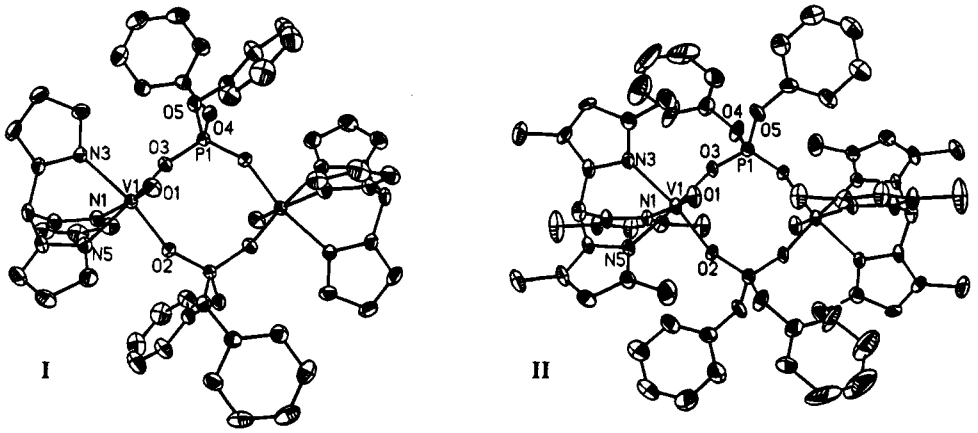

Figure 1. Thermal ellipsoid plot (30%) with atom labels for the dinuclear complex in the structures of $[LVO(\mu\text{-}(C_6H_5O)_2PO_2)]_2$ (**I**) and $[L'VO(\mu\text{-}(C_6H_5O)_2PO_2)]_2$ (**II**). View is perpendicular to the bridging O_4 plane of the dimers. Hydrogen atoms have been omitted to improve clarity.

Table 4. Atomic Coordinates ($\times 10^4$) and Equivalent, Isotropic Thermal Parameters ($Å^2 \times 10^3$) for $[L'VO(\mu\text{-}C_6H_5O)_2PO_2)]_2 \cdot C_7H_8$ (**II**)

atom	x	y	z	U(eq)[a]	atom	x	y	z	U(eq)[a]
V(1)	1(2)	1250(1)	1064(1)	31(1)	N(6)	−970(7)	2883(5)	1155(5)	35(3)
P(1)	1683(2)	−7(2)	392(2)	35(1)	C(17)	−1974(10)	1980(7)	1488(8)	46(4)
O(1)	5(6)	737(4)	1923(4)	46(3)	C(18)	−2421(10)	2709(7)	1554(8)	55(4)
O(2)	−1116(5)	666(4)	162(4)	39(3)	C(19)	−1782(11)	3270(7)	1327(8)	50(4)
O(3)	1095(5)	645(4)	654(4)	37(3)	C(170)	−2364(11)	1175(7)	1694(10)	84(5)
O(4)	2419(6)	326(4)	−163(5)	58(3)	C(190)	−1864(11)	4151(7)	1287(8)	70(5)
O(5)	2416(6)	−315(4)	1295(5)	57(3)	C(21)	3126(10)	945(8)	76(8)	58(4)
B(1)	8(12)	3192(8)	934(8)	43(4)	C(22)	2872(13)	1635(9)	355(12)	108(5)
N(1)	−2(7)	2074(4)	−134(5)	34(3)	C(23)	3557(16)	2267(12)	565(14)	140(6)
N(2)	−1(8)	2882(4)	−7(5)	38(3)	C(24)	4510(19)	2145(15)	552(17)	203(6)
C(11)	12(9)	1966(6)	−990(7)	39(4)	C(25)	4788(12)	1496(13)	93(14)	144(6)
C(12)	26(11)	2705(6)	−1380(8)	55(4)	C(26)	4051(11)	835(10)	−95(13)	121(5)
C(13)	19(11)	3266(6)	−759(7)	49(4)	C(31)	3078(10)	−954(8)	1434(8)	59(4)
C(110)	−5(10)	1176(6)	−1440(7)	58(4)	C(32)	4038(13)	−841(10)	1971(11)	108(5)
C(130)	26(14)	4153(7)	−827(8)	94(5)	C(33)	4728(14)	−1481(11)	2201(13)	136(6)
N(3)	1114(7)	2079(5)	1768(6)	37(3)	C(34)	4446(14)	−2210(10)	1847(13)	119(6)
N(4)	993(8)	2883(5)	1626(5)	36(3)	C(35)	3452(13)	−2334(9)	1289(10)	91(5)
C(14)	1993(10)	1973(7)	2423(8)	50(4)	C(36)	2784(11)	−1678(8)	1081(9)	73(5)
C(15)	2430(9)	2723(7)	2696(8)	51(4)	C(50)	−4656(21)	5676(13)	75(17)	194(8)
C(16)	1786(10)	3265(7)	2175(8)	44(4)	C(51)[b]	−3999(26)	5504(20)	−455(28)	183(10)
C(140)	2388(11)	1192(8)	2781(9)	87(5)	C(52)	−4051(22)	4769(21)	−862(19)	274(9)
C(160)	1896(11)	4151(7)	2211(10)	82(5)	C(53)[b]	−4700(29)	4190(15)	−676(25)	139(9)
N(5)	−1101(7)	2072(5)	1239(5)	36(3)	C(60)[b]	−4745(28)	4959(16)	−374(32)	205(10)

[a] Equivalent isotropic U defined as one-third of the trace of the orthogonalized U_{ij} tensor. [b] Site occupation factors fixed at 0.5.

employing a Bruker NR80 FT-NMR. The solid samples used for variable-temperature magnetic susceptibility measurements were finely powdered and then packed and sealed in gelatin capsule sample holders. Measurements were made in the temperature range 5−270 K on an LDJ 9600 vibrating-sample magnetometer. Temperature was controlled by an Oxford ITC4 set-point controller and cryostat and was measured with a thermocouple located approximately 1.5 cm upstream from the sample. The magnetic moment was calibrated to the saturation moment of a nickel metal standard. Temperature calibration was checked using the magnetic standards $HgCo(SCN)_4$ and $[(CH_3)_2NHCH_2]_2CuCl_4$.[12] A magnetization curve measured at the lowest temperature for each sample was linear with respect to field through the range of field values used in each data collection, thus zero-field susceptibilities were calculated by using the simple relation $\chi = M/H$. Temperature-independent contributions to the paramagnetism were accounted for through an empirical correction obtained from a plot of χ_{raw} versus T^{-1}.

Electrochemistry. Electrochemical measurements were made using a BAS CV-27 electrochemical analyzer. Cyclic voltammetry using Pt bead electrodes was performed as previously described.[13] Dry methylene chloride (Burdick and Jackson Distilled-in-Glass grade) was used as the solvent with tetrabutylammonium hexafluorophosphate as a supporting electrolyte. Potentials were measured vs a Ag/AgCl reference electrode with the ferrocene/ferrocenium couple used as an internal standard.

EPR Spectroscopy. EPR spectra were measured on a Micro-Now 8300A spectrometer. Spectra were measured for all three compounds in the forms of fluid solution, frozen solvent glass (toluene/$MeCl_2$, 77 K), and finely powdered solids. Low-temperature spectra were measured with the aid of a quartz Dewar insert in the microwave cavity and with the magnetic field calibrated against the DPPH resonance spectrum. Representative EPR spectra for the three compounds are presented in Figure 3.

Results

Crystal Structures. (a) $[(L/L')VO(\mu\text{-}(C_6H_5O)_2PO)]_2$, Compounds I/II. These compounds are both found as bis(μ-diphenyl phosphato-*O,O'*) divanadyl complexes and have many structural features in common. Bond lengths and angles about the vanadium and phosphorus atoms show good agreement between the two structures (see Table 3). The vanadium atoms in both systems are found with distorted octahedral coordination geometries. Three of four terminal coordination sites of each metal center are occupied by the hydridotris(pyrazolyl)borate capping ligand (**I**) or the 3,5-dimethylpyrazolyl analog (**II**). The vanadyl oxygen occupies the fourth, terminal site and is oriented

(11) Evans, D. F. *J. Chem. Soc.* **1959**, 2003.
(12) Brown, D. B.; Crawford, V. H.; Hall, J. W.; Hatfield, W. E. *J. Phys. Chem.* **1977**, *81*, 1303.
(13) Bonadies, J. A.; Carrano, C. J. *J. Am. Chem. Soc.* **1986**, *108*, 4088.
(14) Chen, Q.; Salta, J.; Zubieta, J. *Inorg. Chem.* **1993**, *32*, 4485.

Table 5. Atomic Coordinates ($\times 10^4$) and Equivalent, Isotropic Thermal Parameters ($Å^2 \times 10^3$) for $H_2O \subset [t\text{-Bupz}(\mu\text{-}C_6H_5OPO_3)VO]_6(H_2O)_2 \cdot 2CH_3CH_2OH$ (**III**)

atom	x	y	z	U(eq)[a]	atom	x	y	z	U(eq)[a]
V(1)	816(1)	6554(1)	2804(1)	35(1)	C(26)	−2453(5)	3522(10)	2349(5)	57(6)
V(2)	−855(1)	2972(1)	2142(1)	38(1)	C(260)	−2872(6)	4219(11)	2280(8)	87(8)
V(3)	56(1)	5410(1)	3896(1)	35(1)	C(261)	−3246(9)	3968(18)	1873(9)	250(20)
P(4)	−319(1)	3775(2)	3153(1)	37(1)	C(262)	−2660(8)	5072(12)	2170(10)	225(20)
P(5)	−248(1)	7203(2)	3255(1)	36(1)	C(263)	−3153(9)	4272(15)	2705(8)	233(18)
P(6)	1017(1)	4881(2)	3573(1)	37(1)	C(31)	664(5)	6219(5)	4813(4)	54(5)
O(1)	1340(3)	7027(6)	2988(3)	52(3)	C(32)	978(5)	6900(9)	4977(5)	63(6)
O(11)	1134(3)	5556(5)	2425(3)	43(3)	C(33)	1027(5)	7436(9)	4569(5)	51(5)
O(12)	0	5759(6)	2500	37(4)	C(330)	1331(6)	8270(11)	4507(6)	69(7)
O(2)	−761(3)	2048(5)	2398(3)	58(3)	C(331)	1315(7)	8556(12)	3998(6)	135(11)
O(3)	−286(3)	5085(5)	4295(3)	46(3)	C(332)	1126(9)	8977(11)	4819(7)	157(13)
O(41)	−552(3)	3248(6)	3583(3)	57(4)	C(333)	1888(8)	8085(13)	4696(8)	171(14)
O(42)	−233(3)	4730(5)	3314(2)	40(3)	C(41)	−1042	3068	3641	56(6)
O(43)	−713(3)	3789(5)	2709(3)	36(3)	C(42)	−1186(5)	2186(7)	3680(4)	101(9)
O(44)	178(3)	3288(5)	3094(3)	45(3)	C(43)	−1696	1970	3769	142(13)
O(51)	−382(3)	8021(5)	3586(3)	45(3)	C(44)	−2061	2635	3819	174(17)
O(52)	−330(3)	6426(4)	3593(3)	35(3)	O(45)	−1917	3517	3780	159(15)
O(53)	314(3)	7286(5)	3146(3)	37(3)	C(46)	−1408	3733	3690	92(8)
O(54)	−636(3)	7202(5)	2819(3)	42(3)	C(51A)[b]	−267	8905	3515	26(12)
O(61)	1540(3)	5255(5)	3847(3)	48(3)	C(52A)[b]	32(8)	9242(12)	3159(6)	84(11)
O(62)	744(3)	5695(5)	3342(2)	36(3)	C(53A)[b]	152	10138	3153	107(13)
O(63)	1154(3)	4199(5)	3223(2)	36(3)	C(54A)[b]	−28	10699	3504	70(9)
O(64)	666(3)	4566(5)	3954(3)	37(3)	C(55A)[b]	−327	10362	3860	82(10)
N(21)	−1042(4)	2397(6)	1443(3)	41(4)	C(56A)[b]	−446	9466	3865	52(8)
N(22)	−859(4)	2700(6)	1026(3)	41(4)	C(51B)[b]	−325	8880	3473	75(23)
N(23)	−1651(4)	2966(7)	2288(3)	41(4)	C(52B)	−464(8)	9230(16)	3011(8)	83(11)
N(24)	−1973(4)	3670(7)	2206(3)	51(4)	C(53B)[b]	−402	10129	2927	93(13)
N(31)	511(4)	6289(6)	4336(3)	37(4)	C(54B)[b]	−202	10678	3304	109(14)
N(32)	744(4)	7034(6)	4198(3)	41(4)	C(55B)[b]	−63	10329	3765	139(17)
C(21)	−1281(5)	1664(8)	1318(5)	55(6)	C(56B)[b]	−125	9429	3850	78(11)
C(22)	−1263(5)	1479(10)	826(4)	60(6)	C(61)	1833	4805	4205	42(5)
C(23)	−1001(5)	2167(9)	647(5)	45(5)	C(62)	2009(4)	3949(6)	4133(3)	68(6)
C(230)	−819(6)	2343(10)	141(5)	55(6)	C(63)	2311	3518	4505	94(8)
C(231)	−836(7)	3318(10)	21(5)	117(10)	C(64)	2437	3941	4950	94(8)
C(232)	−284(7)	2001(12)	120(6)	121(10)	C(65)	2260	4796	5022	109(9)
C(233)	−1191(7)	1888(11)	−235(5)	105(8)	C(66)	1958	5228	4649	82(7)
C(24)	−1950(6)	2394(10)	2501(5)	61(6)	O(01)	1372(4)	5927(7)	1518(3)	75(4)
C(25)	−2441(6)	2706(10)	2539(5)	69(7)	C(01B)	1710(8)	6428(22)	1410(11)	273(24)
					C(02B)	2181(9)	6389(19)	1359(8)	243(20)

[a] Equivalent isotropic U defined as one-third of the trace of the orthogonalized U_{ij} tensor. [b] Site occupation factors: **A** orientation, 0.518(1); **B** orientation, 0.482(1).

anti with respect to the other vanadyl oxygen, as has been previously observed by Zubieta and co-workers in $[V_2O_2Cl_2(C_6H_5PO_3H)_2(H_2O)_2]$.[14] The remaining two coordination sites of each metal center are filled by oxygen atoms of the two bridging diphenyl phosphate groups which, in turn, link the vanadyl complexes together to produce the dinuclear cluster. Both **I** and **II** have inversion site symmetry, a feature also found in Zubieta's compound, so that only half the molecule is crystallographically unique.

There are, however, some notable discrepancies between the structures of **I** and **II**. The most obvious is the difference in the V···V distances, 4.931(1) Å for **I** versus 5.367(4) Å for **II**. This increase in distance can be attributed to the expansion necessary for the cluster to accommodate the sterically bulky 3,5-dimethylpyrazolyl ligand in **II**. This expansion is further evident in the corresponding increase in the V−O−P bridge angles. For **I**, the unsubstituted pyrazolyl analog, the V−O−P bridge angle is, on average, only about 15° larger than the pendant P−O−C angles ($V-O-P_{mean} = 137.0°$; $P-O-C_{mean} = 123.6°$). In the 3,5-dimethylpyrazolyl analog **II**, on the other hand, the V−O−P bridge angle is over 30° larger than the pendant P−O−C angles ($V-O-P_{mean} = 160.9°$; $P-O-C_{mean} = 127.6°$). However, this bridge angle increase arises not just from a simple expansion of the dimer but also from a flattening of the eight-member ring that constitutes the bridge core. This is shown quite clearly in Figure 4, which depicts the core atoms of both dimers viewed down the P···P axis. Here the central eight-member ring of **I** clearly assumes a chair conformation in which the dihedral angle between the VO_2 and PO_2 planes, 128.4°, is very close to the ideal of 120° found in chair cyclohexane. In contrast, the central eight-member ring of **II**, while showing some tendency toward the chair conformation, is almost flat with the dihedral angles between VO_2 and PO_2 planes, 164.7°, close to the ideal of 180° for a completely planar ring system. The central ring structure is folded in both cases so that the vanadyl oxygen appears to be retracted into the bridging unit as opposed to extending away from it. This is most apparent in system **I**, where this inward direction of the V=O bond combined with the chair conformation of the bridging unit serves to place the vanadyl oxygen very close to (0.284 Å below) the basal plane of the neighboring vanadyl unit.

(b) $H_2O \subset [t\text{-Bupz}(\mu\text{-}C_6H_5OPO_3)VO]_6(H_2O)_2 \cdot 2CH_3CH_2OH$, Compound III. This hexavanadyl cluster contains three distinctly different vanadyl coordination environments. Because of the complexity of the structure, our discussion will focus on the features of the polyvanadyl core at the expense of the peripheral ligation. The cluster is located about a site of 2-fold rotation symmetry; thus only half of the cluster is unique. The three vanadyl coordination polyhedra within the unique portion can be characterized as follows: (i) V(1), a tris(μ-phosphato) μ-aqua vanadyl hydrate with no coordinated pyrazoles; (ii) V(3), a tris(μ-phosphato) *t*-Bupz vanadyl complex in which one phosphate ligand is coordinated in a rare bidentate chelate/

Table 6. Pertinent Bond Lengths (Å) and Angles (deg) for $H_2O\subset[t\text{-Bupz}(\mu\text{-}C_6H_5OPO_3)VO]_6(H_2O)_2{\cdot}2CH_3CH_2OH$ (**III**)

V(1)–V(1A)	4.389(2)	V(1)–V(2)	7.073(2)
V(1)–V(2A)	5.437(2)	V(1)–V(3)	4.112(2)
V(1)–V(3A)	5.305(2)	V(2)–V(2A)	4.666(2)
V(2)–V(3)	6.366(2)	V(2)–V(3A)	5.200(2)
V(3)–V(3A)	7.666(2)	V(1)–O(1)	1.571(8)
V(1)–O(11)	2.051(8)	V(1)–O(12)	2.504(4)
V(1)–O(53)	2.002(8)	V(1)–O(62)	1.993(7)
V(1)–O(54A)	1.996(7)	V(2)–O(2)	1.579(8)
V(2)–O(43)	2.003(7)	V(2)–N(21)	2.129(10)
V(2)–N(23)	2.124(10)	V(2)–O(44A)	1.972(8)
V(2)–O(63A)	2.220(7)	V(3)–O(3)	1.547((8)
V(3)–O(42)	1.992(7)	V(3)–O(52)	1.978(7)
V(3)–O(62)	2.475(7)	V(3)–O(64)	2.022(7)
V(3)–N(31)	2.091(9)		

O(1)–V(1)–O(11)	97.6(4)	O(1)–V(1)–O(12)	178.0(4)
O(11)–V(1)–O(12)	80.4(3)	O(1)–V(1)–O(53)	99.6(4)
O(11)–V(1)–O(53)	162.3(3)	O(12)–V(1)–O(53)	82.3(3)
O(1)–V(1)–O(62)	101.1(4)	O(11)–V(1)–O(62)	87.9(3)
O(12)–V(1)–O(62)	78.7(2)	O(53)–V(1)–O(62)	84.7(3)
O(1)–V(1)–O(54A)	100.4(4)	O(11)–V(1)–O(54A)	89.9(3)
O(12)–V(1)–O(54A)	79.8(3)	O(53)–V(1)–O(54A)	91.1(3)
O(62)–V(1)–O(54A)	158.5(3)	O(2)–V(2)–O(43)	100.9(4)
O(2)–V(2)–N(21)	93.1(4)	O(43)–V(2)–N(21)	166.0(3)
O(2)–V(2)–N(23)	91.4(4)	O(43)–V(2)–N(23)	88.2(3)
N(21)–V(2)–N(23)	91.3(4)	O(2)–V(2)–O(44A)	104.9(4)
O(43)–V(2)–O(44A)	90.0(3)	N(21)–V(2)–O(44A)	86.5(4)
N(23)–V(2)–O(44A)	163.6(4)	O(2)–V(2)–O(63A)	168.6(4)
O(43)–V(2)–O(63A)	82.4(3)	N(21)–V(2)–O(63A)	83.8(3)
N(23)–V(2)–O(63A)	77.8(3)	O(44A)–V(2)–O(63A)	85.9(3)
O(3)–V(3)–O(42)	102.2(4)	O(3)–V(3)–O(52)	104.6(4)
O(42)–V(3)–O(52)	85.7(3)	O(3)–V(3)–O(62)	167.3(3)
O(42)–V(3)–O(62)	80.4(3)	O(52)–V(3)–O(62)	87.9(3)
O(3)–V(3)–O(64)	103.2(4)	O(42)–V(3)–O(64)	88.2(3)
O(52)–V(3)–O(64)	152.2(3)	O(62)–V(3)–O(64)	64.3(3)
O(3)–V(3)–N(31)	96.6(4)	O(42)–V(3)–N(31)	161.2(3)
O(52)–V(3)–N(31)	89.0(3)	O(62)–V(3)–N(31)	81.4(3)
O(64)–V(3)–N(31)	88.0(3)	V(3)–O(42)–P(4)	139.4(5)
V(2)–O(43)–P(4)	133.2(5)	P(4)–O(44)–V(2A)	160.7(5)
V(3)–O(52)–P(5)	140.1(5)	V(1)–O(53)–P(5)	135.9(5)
P(5)–O(54)–V(1A)	141.4(5)	V(1)–O(62)–P(6)	140.0(5)
P(6)–O(63)–V(2A)	142.2(5)	V(3)–O(64)–P(6)	104.6(4)

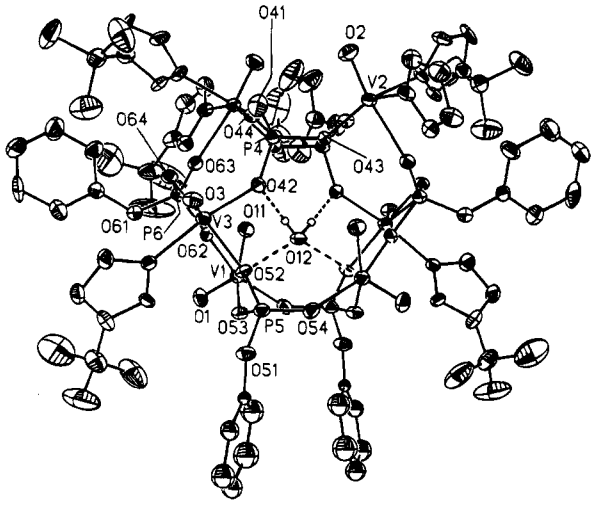

Figure 2. Thermal ellipsoid plot (30%) with atom labels of the structure for the hexanuclear complex in $H_2O\subset[t\text{-Bupz}(\mu\text{-}C_6H_5OPO_3)VO]_6(H_2O)_2{\cdot}2CH_3CH_2OH$ (**III**). View is perpendicular to the mean plane of the cluster. Hydrogen atoms, except those bound to the central water molecule, a phenyl ring, and a *tert*-butyl group have been omitted to improve clarity. The 2-fold rotation axis of the cluster is vertical and in the plane of the page.

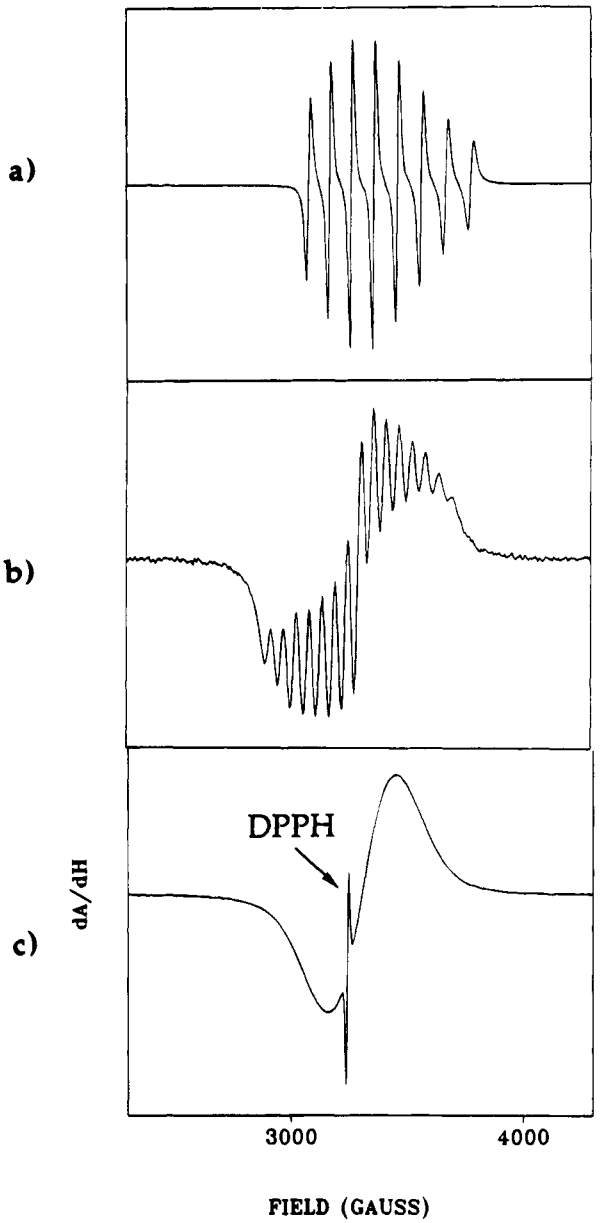

Figure 3. (a) EPR spectrum for **II** in 50% toluene/50%CH_2Cl_2 at 293 K (ν = 9.6 GHz, power = 9 dB, modulation amplitude = 12.5 G, gain = 160). (b) EPR spectrum for **I** in 50% toluene/50%CH_2Cl_2 at 293 K (ν = 9.6 GHz, power = 10 dB, modulation amplitude = 10 G, gain = 500). (c) EPR spectrum for **III** in 50% toluene/50%CH_2Cl_2 at 77 K (ν = 9.2 GHz, power = 11 dB, modulation amplitude = 20 G, gain = 100).

bridging mode; and (iii) V(2), a tris(μ-phosphato) bis(*t*-Bupz) vanadyl species. Symmetry generation of the other half of the cluster produces a vaselike structure in which the symmetry-related pair of V(1) octahedra form the base, the pair of V(3) octahedra define the walls, and the pair of symmetry-related V(2) octahedra form the mouth. The water molecule that bridges between the V(1) pair of octahedra is actually found within the cavity of the "vase" (and on the 2-fold rotation axis). Here each lone pair of the encapsulated water molecule is coordinated to a different V(IV) ion (and *trans* to the vanadyl oxygens) and each hydrogen atom is linked to a bridging phosphate oxygen (H(12)···O(42A) = 1.88 Å, O(12)–H(12)···O(42A) = 180°). Additional hydrogen bonding is provided by the terminal water molecule of V(1), which forms a bifurcated link to O(41) and O(42) that serves to close off the walls of this polyvanadyl vase (H(11B)···O(42A) = 2.48, H(11B)···O(43A) = 2.19 Å, O(11)–H(11B)···O(42A) = 144°, O(11)–H(11B)···O(43A) = 141°, O(42A)···H(11B)···O(43A) = 63°).

Each of the three distinct vanadium(IV) centers is six-coordinate and exhibits the distorted octahedral geometry

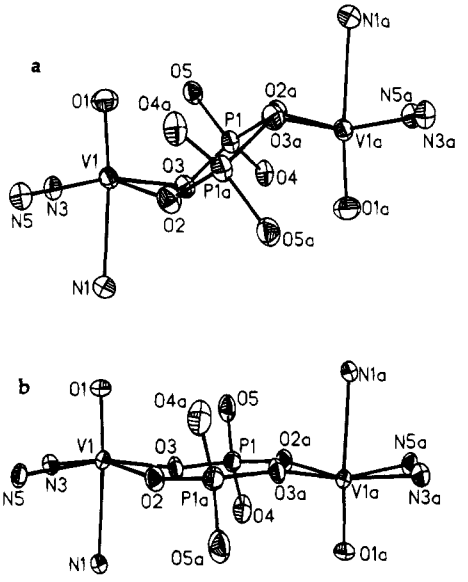

Figure 4. Thermal ellipsoid plots (30%) of the core structures of the dinuclear complexes in (a) $[LVO(\mu\text{-}(C_6H_5O)_2PO_2)]_2$ (**I**) and (b) $[L'VO(\mu\text{-}(C_6H_5O)_2PO_2)]_2$ (**II**).

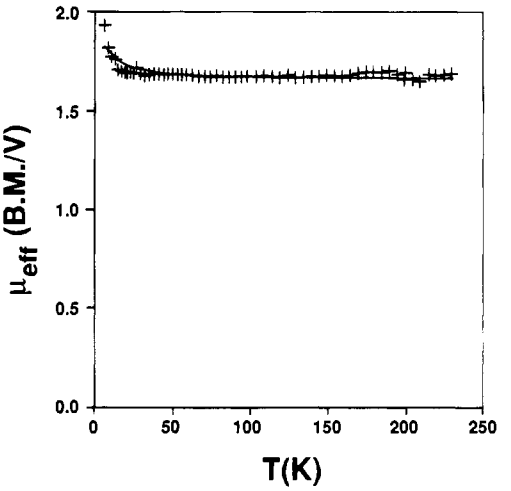

Figure 5. Plot of μ_{eff} versus temperature for $[LVO(\mu\text{-}(C_6H_5O)_2PO_2)]_2$, **I**: +, experimental data; —, theoretical fit to the Bleaney–Bowers equation.

expected for a vanadyl complex. Axial V=O bond lengths (1.566(8) Å) are considerably shorter than other coordination bond lengths and generate a pronounced lengthening of the bonds *trans* to them: $V(1)-O(12)_{water}$ 2.504(4) Å, $V(2)-O(63A)_{phosphate}$ = 2.220(7) Å, and $V(3)-O(62)_{phosphate}$ = 2.475(7) Å. Equatorial coordination bond lengths lie between these extremes: $V-O_{mean}$ = 2.001(7) Å and $V-N_{mean}$ = 2.115(10) Å. The pronounced difference in length between the two *trans* $V-O_{phosphate}$ bonds listed above arises because of the unusual bidentate chelate/bridging role assumed by the P(6) phosphate ligand. In this situation, both O(62) and O(64) are coordinated to V(3) with O(62) located *trans* to the vanadyl oxygen while O(62) also coordinates V(1) in an equatorial position. The unusually large *trans* V(3)–O(62) bond length can thus be attributed to some combination of bridge formation and the strain associated with chelation. This strain is most apparent in the value of the O(62)–V(3)–O(64) angle, 64.3(3)°, which is substantially smaller than the ideal of 90°.

The ester P–O bond lengths are all significantly larger than the non-ester bonds, 1.591 Å versus 1.512 Å, respectively, but the greater range in distribution of the non-ester bonds (1.476–1.532 Å) reflects the wider variety of bonding environments found for the non-ester phosphate oxygens. The largest non-ester P–O bond is found for O(62), a bond that is expected to be the weakest since this is the only phosphate oxygen that coordinates two different metal centers. Conversely, the smallest non-ester P–O bond is found for O(63), a bond which is expected to be the strongest since O(63) only coordinates a single metal center *trans* to a vanadyl oxygen resulting in a weak metal–oxygen interaction.

The peripheral ligands radiate away from the cluster core but only from the base and walls. The mouth of the vaselike cavity is, however, relatively open; the only obstructions are the two vanadyl oxygens which project up from the edges. Two solvated ethanol molecules are also found packed with the other peripheral ligands along the side of the cluster and appear to be held in place by a weak hydrogen bond between the ethanolic hydrogen and a vanadyl oxygen.

Magnetic Measurements. Variable-temperature magnetic susceptibility data for both the dinuclear cluster $[LVO(\mu\text{-}(C_6H_5O)_2PO_2)]_2$ (**I**) and the hexanuclear cluster $H_2O\subset[t\text{-Bupz}(\mu\text{-}C_6H_5OPO_3)VO]_6(H_2O)_2{\cdot}2CH_3CH_2OH$ (**III**) show a monotonic increase with decreasing temperature. Data in the higher temperature regions exhibit Curie-like paramagnetic behavior, but data for both compounds exhibit deviations from the Curie law at lower temperature. Since these metal cluster cores are surrounded by a sheath of organic groups, they should be well isolated from neighboring clusters. Thus, deviations from Curie-like behavior almost certainly arise from intracluster coupling.

For the vanadyl dinuclear species, **I**, a plot of effective magnetic moment versus temperature is essentially level throughout most of the temperature range with a smoothly increasing "tail" rising above this level at the lowest temperatures. We ascribe this behavior to weak ferromagnetic intradimer coupling, and indeed, the Bleaney–Bowers[15] equation gives a reasonable fit to the data (Figure 5) with J/k = 3.3(4) K and g = 1.918(5).

Effective moment data for the hexanuclear cluster, on the other hand, show a pronounced downturn at lower temperatures that is indicative of antiferromagnetic coupling. Within the hexanuclear cluster the 2-fold rotation symmetry renders nine independent coupling constants for the fifteen pairwise coupling terms in the HDVV spin Hamiltonian. We have avoided development of this model, however, because even with the aid of symmetry it would be a laborious process of doubtful utility. Fitting the smooth, slowly varying moment data to such a model would lead to a great deal of correlation and uncertainty in the nine or more parameters. Thus we have undertaken to fit the data to two simple models, each with a single independent coupling constant, that represent extreme situations. The spin Hamiltonian for the first model is expressed

$$\mathcal{H} = -2J(\mathbf{s}_1{\cdot}\mathbf{s}_{1A} + \mathbf{s}_2{\cdot}\mathbf{s}_{2A})$$

and ignores all spin–spin coupling except for that between two pairs of spins (presumably the symmetry-related pairs at the mouth and base of the vaselike structure in Figure 2). The fit of this model, shown in Figure 6, with J/k = −14.4(3) K and g = 1.874(3) agrees very well with the data. Refinement of a similar model with two independent coupling constants yields a marginally better fit but also a high degree of correlation between the coupling parameters and an average coupling constant that is identical to that of the first model, within error. In the opposite extreme, we have considered a model which includes coupling between all spin pairs in the cluster, albeit with the same coupling constant for every pair, and is expressed

(15) Bleaney, B.; Bowers, K. D. *Proc. R. Soc. London* **1952**, *A214*, 451.

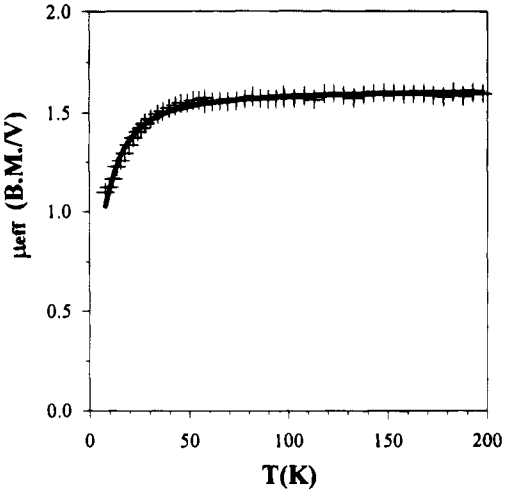

Figure 6. Plot of μ_{eff} versus temperature for $H_2O\subset$[*t*-Bupz(μ-$C_6H_5OPO_3$)VO]$_6(H_2O)_2$·$2CH_3CH_2OH$, **III**: +, experimental data; —, theoretical fit to an isolated dimers model; see text.

by the spin Hamiltonian

$$\mathcal{H} = -2J(\mathbf{S}^2 - \sum_i \mathbf{s}_i^2)$$

i varies through the six metal sites of the cluster. A fit of the data to this model with $J/k = -3.3(1)$ K and $g = 1.901(6)$ gives good agreement, although poorer than for the first model (the root sum of squares is 0.347 for the second model as opposed to 0.239 for the first). It would appear, then, that the coupling between two spin pairs dominates over that arising from other pairwise interactions.

EPR Spectroscopy. The EPR spectrum for **I** dissolved in 50% toluene/50% CH_2Cl_2 at 20 °C, shown in Figure 3b, is the typical 15-line spectrum ($g = 1.962$, $A = 0.005\,12$ cm^{-1}) expected for an exchange-coupled divanadyl complex.[16] The corresponding spectrum at 77 K shows a greater than 15-line spectrum that results from the overlap of the 15-line patterns associated with the two different EPR transitions within the spin triplet of the dimer. The splitting of these two transitions typically arises from the dipolar interactions between the two spins of a vanadyl dimer. Poor peak resolution in the 77 K spectrum of **I**, however, prevents accurate determination of the zero-field splitting parameter. Measurement of the spectrum in DMF, on the other hand, yields an eight-line spectrum characteristic of a monomeric vanadium complex,[17] much like that in Figure 5a, leading us to believe that the dimer dissociates in the much more polar solvent. The spectrum of the solid at room temperature consists of a broad, almost unstructured, Gaussian line ($\Delta H_{pp} = 420$ G).

Compound **II** exhibits in 50% toluene/50% CH_2Cl_2 solution an eight-line EPR spectrum (Figure 3a; $g = 1.982$, $A = 0.009\,22$ cm^{-1}), such as that shown by **I** in DMF, characteristic of a mononuclear vanadyl complex but in contrast to the 15-line dinuclear spectrum shown by **I** in the same solvent. This eight-line spectrum persists in pure toluene, a solvent with a small dielectric constant and in which the compound is only sparingly soluble. At 77 K in a 50% toluene/50% CH_2Cl_2 glass, compound **II** exhibits an anisotropic eight-line spectrum ($g_{||} = 1.947$, $A_{||} = 0.0162$ cm^{-1}; $g_\perp = 1.986$, $A_\perp = 0.005\,80$ cm^{-1}) with none of the zero-field splitting effects associated with other divanadyl species. A spectrum of the powdered solid at room temperature reveals a single broad Gaussian line ($\Delta H_{pp} = 350$ G) with some ill-resolved structure that is perhaps related to the underlying hyperfine pattern or to anisotropy in the *g* factor.

In contrast to those of the previous two compounds, the EPR spectrum of compound **III** (Figure 3c) shows in all cases just a single broad, unstructured line. At room temperature in 50% toluene/50% CH_2Cl_2 solution the line is primarily Gaussian ($g = 1.960$, $\Delta H_{pp} = 250$ G) and changes little upon reducing the temperature to 77 K ($g = 1.966$, $\Delta H_{pp} = 290$ G with 21% Lorentzian character). The room-temperature solid-state spectrum agrees well with the solution results ($g = 1.958$, $\Delta H_{pp} = 270$ G with 19% Lorentzian character), suggesting that intercluster magnetic interactions are almost negligible in the solid.

Electrochemistry. The hydridotris(pyrazolyl)borate divanadium complex, **I**, is oxidized at +1.45 V versus Ag/AgCl, while the value for the 3,5-dimethyl derivative is +1.15 V. That the 3,5-dimethyl derivative is easier to oxidize than the unsubstituted analog is in keeping with the greater electron-donating power of the former. However, the −0.3 V stabilization is moderately larger than has been previously reported for analogous tris(pyrazolyl)borate complexes of vanadium.[7]

Surprisingly, both [LVO(μ-$(C_6H_5O)_2PO_2$)]$_2$ and [L′VO(μ-$(C_6H_5O)_2PO_2$)]$_2$ give quasireversible oxidative electrochemistry on Pt in methylene chloride—surprising because vanadyl species usually give irreversible electrochemistry since either oxidation or reduction typically results in a concurrent chemical change, i.e. gain or loss of an oxo group. The quasireversibility of these systems demonstrates that the dimeric unit remains intact upon oxidation and that the monooxovanadium(V) moiety is stable in the presence of phosphate. This is borne out by the observation of phosphate-bridged monooxovanadium(V) moieties of similar structure in a number of well-characterized organophosphate clusters.[18] The 3,5-dimethyl derivative is the more reversible of the two; i.e., it has a scan rate-invariant i_{pa}/i_{pc} very nearly equal to 1, while for the unsubstituted complex i_{pa}/i_{pc} varies with scan rate (0.65 at 50 mV/s versus 0.85 at 300 mV/s). This increase in kinetic stability for the 3,5-dimethyl derivative *vis à vis* its unsubstituted counterpart has been observed before and is attributed to the reduced accessibility of the metal center in the former complex.[7]

Discussion

The difference between the core structures of the two dinuclear complexes illustrates the relative ease with which the central bridging (O=V)(OPO)$_2$(V=O) ring can be distorted. The central ring in [LVO(μ-$(C_6H_5O)_2PO_2$)]$_2$, **I**, assumes the (presumably) lower energy *chair* conformation while that in [L′VO(μ-$(C_6H_5O)_2PO_2$)]$_2$, **II**, takes a higher energy *quasi-planar* conformation. This distortion from the chair to the planar conformation can be readily accounted for using steric arguments. The presence of the hydridotris(3,5-dimethylpyrazolyl)borate capping ligand L′ in **II**, instead of the unsubstituted pyrazole analog L, forces expansion of the central ring in order to accommodate the sterically bulky methyl groups. Ring expansion could occur *via* a number of different routes, but flattening of the central ring probably gives the largest increase in intermetal separation with the smallest increase in angle strain. One might also expect that a weaker force imposed on the ring would induce a smaller distortion of the chair structure. Thus a continuous range of conformations between chair and planar geometries is possible. Examination of several vanadyl phosphate and sulfate compounds containing this bridging ring

(16) Hahn, C. W.; Rasmussen, P. G.; Bayon, J. C. *Inorg. Chem.* **1992**, *31*, 1963.
(17) Collison, D.; Eardley, D. R.; Mabbs, F. E.; Powell, A. K.; Turner, S. S. *Inorg. Chem.* **1993**, *32*, 664.
(18) Chen, Q.; Zubieta, J. *Angew. Chem., Int. Ed. Engl.* **1993**, *32*, 261. Chang, Y.-D.; Salta, J.; Zubieta, J. *Angew. Chem., Int. Ed. Engl.* **1994**, *33*, 325.

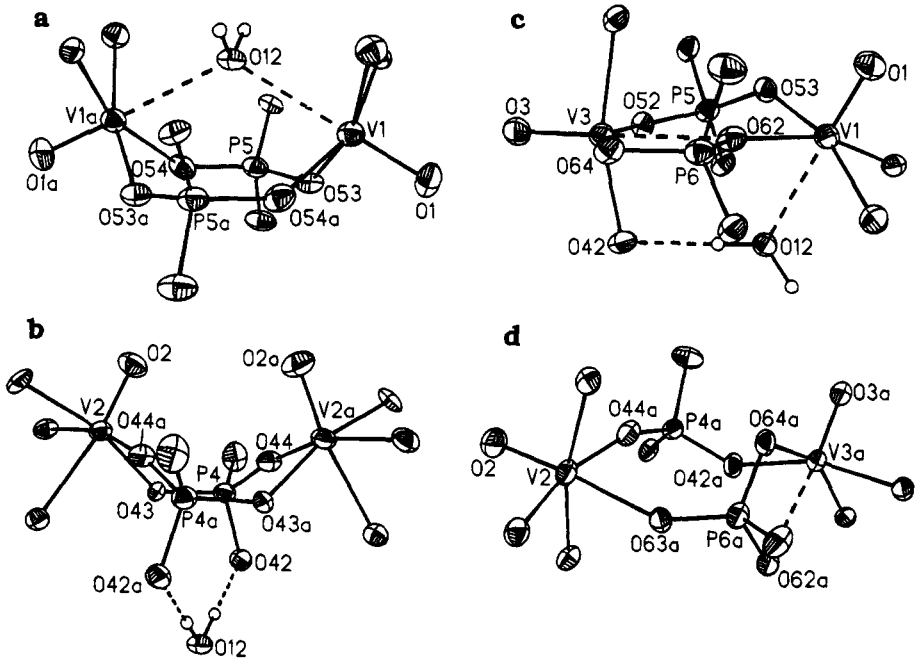

Figure 7. Thermal ellipsoid plots of the core structures for the four unique dimeric components of the hexanuclear cluster in $H_2O\subset[t\text{-Bupz}(\mu\text{-}C_6H_5OPO_3)VO]_6(H_2O)_2{\cdot}2CH_3CH_2OH$ (**III**).

structure confirms that the bridging unit conformation is not confined to the extremes of the chair or planar structures (see below).

The complexity of the hexanuclear cluster, compound **III**, prevents a simple explanation for the differing $(O{=}V)(OPO)_2(V{=}O)$ ring structures present. Optimization of bonding to the central template molecule, in this case a molecule of water, would clearly play a major role in determining the structure of the vanadium phosphate moieties surrounding it. This factor appears to be most important in producing the conformation of the $(O{=}V(1))(OPO)_2(V(1A){=}O)$ ring at the base of the cluster. This ring is found in a *convex boat* conformation with vanadyl oxygen located beneath the keel of the boat and radiating away from the center of the cluster (see Figure 7a). Assumption of this ring conformation enables the two vanadyl cations to be coordinated *trans* to their oxo groups by the two lone pairs of the central water molecule. The bridging $(O{=}V(2))(OPO)_2(V(2A){=}O)$ ring at the mouth of the cluster also assumes a boat conformation that apparently optimizes interactions with the template molecule (see Figure 7b). Here the (twisted) boat conformation can be described as a *concave boat* conformation because the vanadyl oxygens now extend above the hull of the boat. In this instance the concave orientation of the boat allows the protons of the central water molecule to hydrogen-bond to bridging phosphate oxygens located on the boat's keel. Adoption of this conformation also leaves the positions *trans* to the vanadyl oxygens open for bridge bonding to metal centers below, so template interactions are not the sole consideration in determining the conformation of this dinuclear unit.

Two more types of $(O{=}V)(OPO)_2(V{=}O)$ rings are found in cluster **III**, but the forces determining their observed conformations are more difficult to discern than in the previous two. The eight-membered $(O{=}V(1)(OPO)_2(V(3){=}O)$ (see Figure 7c) is unusual in that the phosphate oxygens coordinate one vanadyl center in equatorial *cis* positions but coordinate the other vanadyl center in equatorial *trans* positions. Another interesting feature is the bidenate chelation of V(3) by one of the bridging phosphates, the second phosphate oxygen coordinating V(3) in an axial position. While the template molecule interacts with members of this ring (a lone pair coordinates V(1) and a proton hydrogen-bonds to O(42)), the unusual features of the ring geometry are not directly connected to the central water molecule. Hence the conformation distortion of this bridging unit is influenced largely by requirements for cluster connectivity. The fourth bridging ring type, $(O{=}V(2))(OPO)_2(V(3A){=}O)$, is found with vanadium(IV) ions coordinated by phosphate oxygens at *cis* positions (Figure 7d). However, at one metal center (V(2)) one phosphate coordinates an axial position and the other an equatorial. The origin of this unusual bridging geometry also must arise primarily from cluster connectivity requirements since there is little direct interaction with the central template molecule.

The hexanuclear cluster, **III**, is a prime example of a vanadyl phosphate system that pieces together a diverse array of structural elements into a compact and highly organized framework. But it is not the only example. Recent years have seen the synthesis and characterization of many vanadyl phosphate compounds, in the form of both extended solids and discrete, template-centered clusters, to which this description could also apply.[19-29] Systematic analysis of the occurrence and variability of the common structural components of these

(19) Salta, J.; Chen, Q.; Chang, Y.-D.; Zubieta, J. *Angew. Chem., Int. Ed. Engl.* **1994**, *33*, 757.
(20) Koppen, M.; Fresen, G.; Wieghardt, K.; Llusar, R. M.; Nuber, B.; Weiss, J. *Inorg. Chem.* **1988**, *27*, 721.
(21) Khan, M. I.; Chang, Y.; Chen, Q.; Hope, H.; Parking, S.; Goshorn, D. P.; Zubieta, J. *Angew. Chem., Int. Ed. Engl.* **1992**, *31*, 1197.
(22) LeBail, A.; Percy, G.; Amoros, P.; Beltran, D. *Eur. J. Solid State Inorg. Chem.* **1989**, *26*, 419.
(23) Lii, K.-H.; Wu, L.-S.; Gau, H.-M. *Inorg. Chem.* **1993**, *32*, 4153.
(24) Leoniwicz, M. E.; Johnson, J. W.; Brody, J. F.; Shannon, H. F., Jr.; Newsam, J. M. *J. Solid State Chem.* **1985**, *56*, 370.
(25) Kang, H. Y.; Lee, W. C.; Wang, S. L.; Lii, K. H. *Inorg. Chem.* **1992**, *31*, 4743.
(26) Soghomonian, V.; Haushalter, R. C.; Chen, Q.; Zubieta, J. *Angew. Chem., Int. Ed. Engl.* **1994**, *33*, 1700.
(27) Tachez, P. M.; Theobald, F. *Acta Crystallogr., Sect. B* **1980**, *36*, 2873.
(28) Haushalter, R. C.; Mayer, L.; Dhingra, S. S.; Thompson, M. E.; Wang, Z.; Zubieta, J. *Inorg. Chim. Acta* **1994**, *218*, 59.
(29) Khan, M. J.; Zubieta, J. *Angew. Chem., Int. Ed. Engl.* **1994**, *33*, 760.

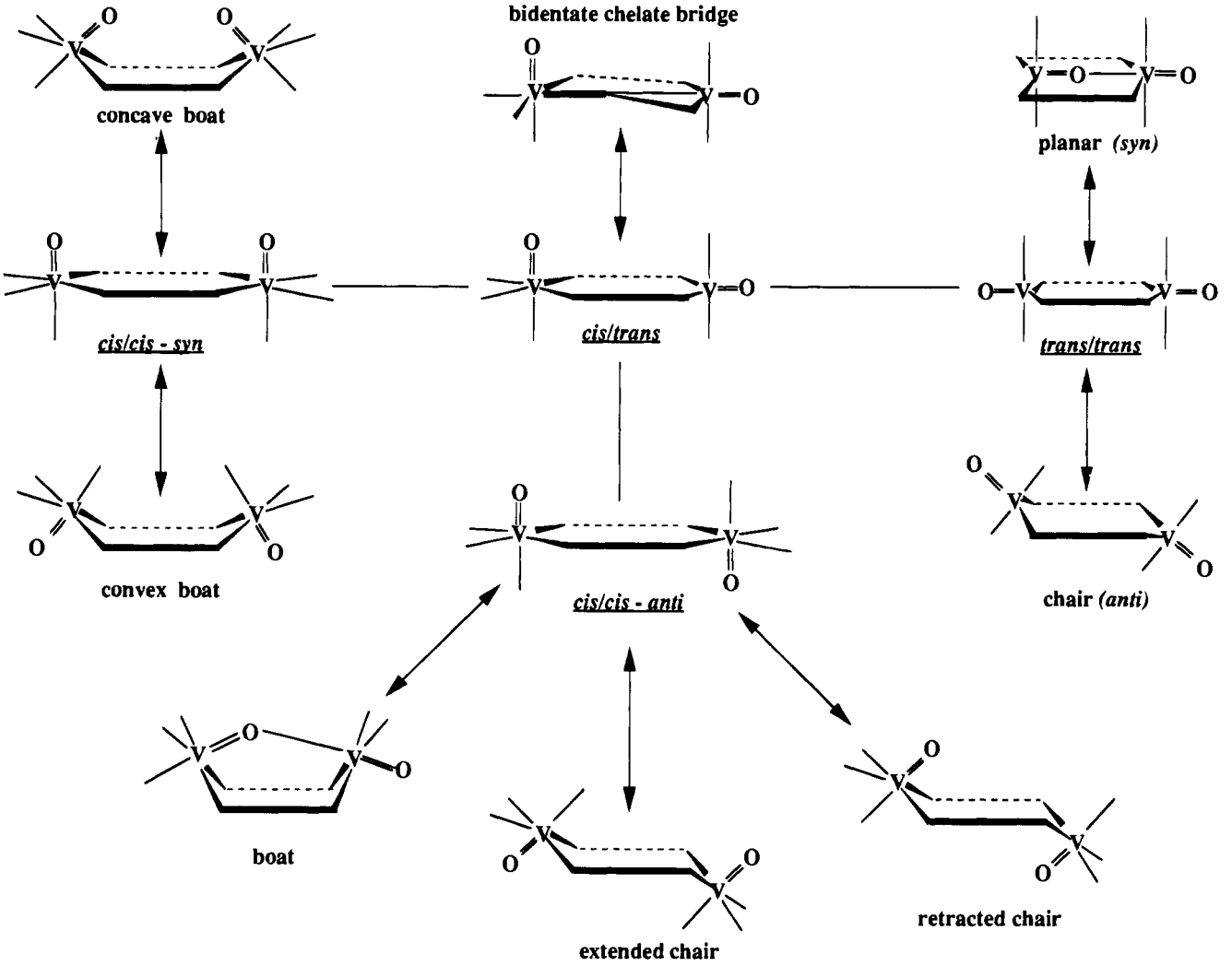

Figure 8. Classification scheme for cyclic $(O{=}V)(OPO)_2(V{=}O)$ bridging units in vanadyl phosphate systems. Names for the four major ring configurations are underlined and appear next to their archetype structures. Archetype structures that differ by the coordination mode at a single vanadium center are connected by a straight line. Double-headed lines connect a given archetypal configuration to the conformations that can be achieved through a continuous bending distortion.

systems is, however, lacking. Beltran-Porter and co-workers[30] have identified several different types of bridging modes found in vanadium phosphate systems and noted their characteristic magnetic exchange properties. We desire to proceed beyond this *ad hoc* approach toward a systematic classification of bridging unit types that will not only identify them but also describe their interrelationships. One of the more predominant structural features is the cyclic $(O{=}V)(OPO)_2(V{=}O)$ bridging unit that is so prominent in the three compounds reported here. Extending our discussion of the properties of this bridging unit to the broader family of vanadyl phosphates, we have developed a systematic scheme for classifying the different types of $(O{=}V)(OPO)_2(V{=}O)$ bridging rings occurring in these systems and have identified some of the major distortion pathways that lead from one bridging conformation to another.

Four major classes of $(O{=}V)(OPO)_2(V{=}O)$ bridging rings form the basis of this classification scheme. These are identified first by the positions, either *cis* or *trans*, that the bridging phosphate oxygens occupy in the equatorial planes of the metal centers. Thus one can find dimeric bridging units with *cis* coordination at both metal centers, *trans* coordination to both, or *cis* to one and *trans* to the other. A further distinction is made for those dimeric species with *cis/cis* coordination by denoting the orientation of the vanadyl oxygens, either *syn* or *anti*, relative to each other. Figure 8 presents the full classification scheme with the *cis/trans* configuration occupying the central position by virtue of the fact that the other three configurational families—*cis/cis-syn*, *cis/cis-anti*, and *trans/trans*—can be derived from this by changing the coordination about one of the metal centers. Within each of these configurations there is a series of different ring conformations that can be achieved by a continuous bending deformation of the parent configuration. We have depicted a number of the possibilities in Figure 8, and we have tried to make this scheme sufficiently comprehensive to include all known and some potential ring geometries. The rationale behind this scheme is general enough, however, that it should be able to extend to any new ring geometries in which all four bridging oxygens coordinate the equatorial planes of the metals. In devising this scheme, we have assumed the orientation about the phosphorus atoms to be fixed. While lateral bending of the phosphate tetrahedra can produce additional ring puckering, phosphorus atoms are more commonly found close to the plane of the bridging oxygens. By ignoring these phosphate distortions, we effectively consider a six-vertex ring as the bridging unit in these dimeric species. This said, one can also generalize the description to include

(30) Beltran-Porter, D.; Amoros, P.; Ibanez, R.; Martinez, E.; Beltran-Porter, A.; Le Bail, A.; Ferey, G.; Villeneuve, G. *Solid State Ionics* **1989**, *32/33*, 57.

systems with similar μ-(O,O) bridging ligands, e.g. arsenates or carboxylates.

The *cis/cis-syn* configurational family, depicted at the far left in Figure 8, contains the two different boat conformations, convex and concave (Figure 7a,b), that appear at the mouth and the base of hexanuclear cluster **III**. Of the two, the convex boat conformation is the more common among template-centered clusters since it places the two vanadyl ions in a position to be easily coordinated *trans* to their vanadyl oxygens by a central template molecule. In this regard, it is interesting to note in the recently determined structure of $Cl\subset(VO)_6(t\text{-}BuPO_3)_8$ that the encapsulated chloride ion is completely surrounded by a quasispherical shell of fused convex boat $(O{=}V)(OPO)_2(V{=}O)$ rings, enabling each vanadyl ion to be coordinated axially by the central chloride.[19] In cluster **III**, on the other hand, the two lone pairs of the less-symmetric water template require just a single convex boat conformation in the cluster framework. The rarer concave boat conformation is found, to our knowledge, in only one other system, $[L^*_2V_2O_2(\mu\text{-}CH_3CO_2)_2]I_2$ (L^* = 1,4,7-trimethyl-1,4,7-triazacyclononane).[20] In this latter compound, the boat conformation is regular in contrast to the twisted boat conformation found in **III**.

The *cis/trans* configuration, obtained from the *cis/cis* configuration by changing the coordination of one vanadyl to *trans*, appears to be quite rare. The *cis/trans* configuration found in **III** (Figure 7c) is the only example of which we are aware. In this particular example, one of the phosphate groups folds into the ring to produce the bidentate bridging mode described above. Folding the phosphate group into the ring allows one of the phosphate oxygens to coordinate both metal centers, one in an equatorial position but the other in an axial position.

The *trans/trans* configuration likewise appears to be rare. We know of only one example, and this is found in the mixed-valence (V(IV)/V(V) cluster $[H_2\{V_6O_{10}(O_3AsC_6H_5)_6\}]^{2-}$.[21] In this example, the vanadyl oxygens are oriented *anti* to one another and there is a moderate distortion of the bridging ring toward a chair conformation. An intriguing *trans/trans* ring structure would be obtained from the parent planar conformation by rotating one of the vanadyl groups about the *trans* O−V−O axis toward a *syn* orientation of the vanadyl oxygens that terminates in V=O···V=O head-to-tail bonding. Although this conformation has not been observed, its analog in the *cis/cis-anti* family has recently been found (see below).

The remaining major class of bridging ring conformations is those with *cis* coordination of the vanadyl centers by the phosphate oxygens and with an *anti* orientation of the vanadyl oxygens. The planar ring conformation, the central archetype from which the other conformations are derived through various bending distortions, is practically realized in dinuclear complex **II**. The relatively common chair conformations can be derived from this ring by folding in one of two ways. In the first, the ring is folded so that the vanadyl oxygens extend away from the ring structure leading to an *extended chair* conformation. An example of this dimeric structure is found in α-$VO(HPO_4)\cdot 2H_2O$.[22] In the second type of chair structure, the ring is folded with the orientation of the vanadyl oxygens reversed so that they appear retracted into the ring. This *retracted chair* conformation is assumed by dinuclear complex **I**. Several other vanadium phosphate structures contain this conformation, but with differences in the degree of distortion to the chair geometry. A sampling of such structures yields the following values for the average dihedral angle between the VO_2 planes of the ring and the bridging O_4 plane: 111.3° ($Ni_{0.5}VOPO_4\cdot 2H_2O$),[23] 117.7° ($VO(HPO_4)\cdot 4H_2O$),[24] 120° (chair cyclohexane), 127.0° ($Co(VO)_2(PO_4)\cdot 4H_2O$),[25] 129.7° (**I**), 130.9° $\{(H_2NC_4H_8NH_2)[(VO)_2(PO)_4)_2]\}$,[26] 131.4° ($VOSO_4\cdot 3H_2O$),[27] 164.7° (**II**), 180° (planar). A dihedral angle of approximately 130° appears to be most common, but there are values substantially larger and smaller than this, suggesting that the chair conformation can easily flex in response to structural forces. The final example of a *cis/cis-anti* conformation is a boat structure that terminates in head-to-tail V=O···V=O bonding. This structural element was recently found as part of a chain (···V=O···V=O···) in the mixed-valence V(IV)/V(V) compound $(NH_4)_3[(VO)(V_2O_3)(AsO_4)_2(HAsO_4)]$.[28] Of even further interest, a ring structure intermediate between the planar and the head-to-tail boat conformation was recently observed in $[2H_2O\subset V_{12}(OH)_2(H_2O)_2(C_6H_5AsO_3)_{10}(C_6H_5AsO_3H)_4\cdot 6H_2O$.[29] In this structure, the boat conformation of the ring is clear, but the ends of the boat are not sufficiently bent together to produce head-to-tail V=O···V=O bonding.

One goal of the systematic classification of the divanadyl structural components of these compounds is to develop a correlation between structural geometry and magnetic exchange interaction. Superexchange interactions through the bridging phosphate are generally weak, although in certain optimal geometries they can be quite strong.[31] Direct exchange is, however, an important and often dominant source of spin−spin interaction. Direct overlap between metal d_{xy} orbitals in the *cis/cis-syn* concave boat conformer $L^*_2V_2O_2(\mu\text{-}CH_3CO_2)_2$ (see **A**), for example, has been invoked to explain the strong

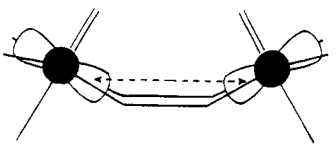

A

antiferromagnetic coupling in this dimer.[20] Similar overlap between these orbitals in the two *cis/cis-syn* boat conformers of hexanuclear cluster **III** would also account for the antiferromagnetic coupling in that compound. Here the magnetic data, which are more easily fit to a model consisting of a pair of isolated dimers, and the EPR signal, the broad Gaussian line indicative of very weak extended exchange interactions, point to strong exchange only in an isolated pair of dimers within the cluster. The two *cis/cis-syn* boat dimers at the base and mouth of the cluster have two of the shortest V···V distances in the cluster[32] (V(1)···V(1A) = 4.389 Å, V(2)···V(2A) = 4.666 Å), and the *cis/cis-syn* boat conformation of the two would be amenable to antiferromagnetic exchange through direct overlap as shown in **A**. The average exchange coupling in these dimers is several times smaller than in the bis(μ-carboxylato) analog, consistent with the shorter V···V distance (4.075 Å) in the latter.

Beyond determination of the types of magnetic exchange typical of a given static geometry, the more interesting question to consider is how that coupling will vary along one of the distortion pathways depicted in Figure 8. For example, dinuclear complexes **I** and **II** lie on the same distortion pathway with **I** taking the *cis/cis-anti* retracted chain conformation while **II** is much closer to the planar archetype. The weak ferromagnetic coupling observed in **I** is at first surprising but can be rationalized in terms of direct exchange. In the retracted chair

(31) Villeneuve, G.; Suh, K. S.; Amoros, P.; Casan-Pastor, N.; Beltran-Porter, D. *Chem. Mater.* **1992**, *4*, 108.

(32) The V(1)···V(3) distance is the shortest (4.111 Å), but direct overlap in this dimeric unit would generate a ferromagnetic interaction because the V=O axes, and hence the magnetic orbitals of the two metals, are almost orthogonal.

conformation, the vanadyl oxygen of one metal center lies close to, but slightly below, the equatorial plane of the opposite center. With this geometry, the unpaired electron in the d_{xy} orbital of one metal can delocalize by direct overlap into the V=O π-system of the other (see **B**). Since the V=O π-orbital is

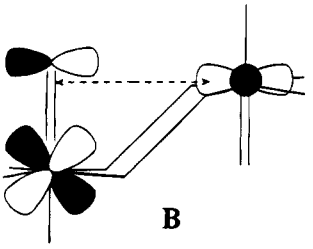

B

orthogonal to its own magnetic orbital, the resulting exchange coupling would be ferromagnetic. As the retracted chair geometry is bent back toward the planar archetype, the d_{xy}–V=O-π overlap will decrease while the d_{xy}–d_{xy} overlap will increase. Overlap of the two vanadyl magnetic orbitals (see **C**) results in antiferromagnetic coupling. Flattening the chair structure also increases the V···V distance and would diminish the magnitude of the magnetic exchange arising from direct interaction. EPR results for complex **II** in solution are characteristic of an uncoupled spin system. One might speculate the lack of coupling in **II** results from its proximity to a crossover point from ferro- to antiferromagnetic coupling. The

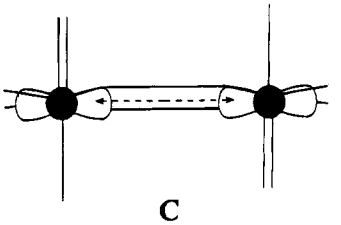

C

V···V distance in **II** is, however, over 0.4 Å larger than in **I** (5.369(4) versus 4.931(1) Å) and the uncoupled nature of the dimer might well result from loss of overlap due to spatial isolation of the two metal centers of the dimer.

Acknowledgment. This work was supported by Grant AI-1157 from the Robert A. Welch Foundation, Grant 3615-002 from the Texas Advanced Research Program, and Area Grant GM4767601 from the NIH to C.J.C. NSF-ILI Program Grant USE-9151286 is acknowledged for support of the X-ray diffraction facilities at Southwest Texas State University.

Supplementary Material Available: Tables of bond lengths and angles, anisotropic thermal parameters, and hydrogen atom positions and isotropic thermal parameters for compounds **I**, **II** and **III** and a disorder description and stereoview for **III** (15 pages). Ordering information is given on any current masthead page.

IC940959L